ACS Photonics 4.3 (2017): 600-605

DOI: https://doi.org/10.1021/acsphotonics.6b00941

Optical identification of few-layer antimonene crystals

Pablo Ares,[†] Felix Zamora,[‡,§,⊥] and Julio Gomez-Herrero*[†§]*

[†]Department of Condensed Matter Physics, Universidad Autónoma de Madrid, E-28049 Madrid, Spain.

[‡]Department of Inorganic Chemistry, Universidad Autónoma de Madrid, E-28049 Madrid, Spain.

[§]Condensed Matter Physics Center (IFIMAC), Universidad Autónoma de Madrid, E-28049, Madrid, Spain.

[⊥]Instituto Madrileño de Estudios Avanzados en Nanociencia (IMDEA-Nanociencia), Cantoblanco, E-28049, Madrid, Spain.

KEYWORDS Antimonene, optical microscopy, atomic force microscopy, refractive index.

ABSTRACT On-surface isolation of few-layer antimonene by micromechanical exfoliation leads to nano-flakes with a variety of thicknesses. Whereas Raman spectroscopy fails to provide information, the optical properties of the antimonene thin flakes allow a simple and quite accurate identification of the different thicknesses based on the optical contrast. We measure the

optical contrast of flakes using different illumination wavelengths in the visible spectrum, and their thickness using atomic force microscopy. The optical contrast is then quantitatively accounted for by a Fresnel-law-based model yielding the refractive index and absorption coefficient of these thin crystals in the visible spectrum. Hence, the optical microscopy data can be quantitatively analyzed to determine the thickness of the flakes in a fast and nondestructive way useful for future nanodevices fabrication.

The experimental isolation of graphene, just a single atomic layer of graphite, by micromechanical exfoliation[1] triggered the rising of a whole new family of 2D materials.[2,3] Among the last isolated are phosphorene[4,5] and antimonene,[6-9] a single atomic layer of phosphorus and antimony, respectively. Both share a similar band gap of ~ 1 eV (for the antimonene case only predicted). Antimonene shows, in comparison with black phosphorus, outstanding stability under ambient conditions.[6-9] Theoretical calculations predict different interesting properties for this material: an electronic structure with a bandgap in the ultrafast optoelectronics applications range,[6,10,11] high carrier mobilities,[12,13,14] topological behavior[15,16] and optical properties[17,18] that would make antimonene suitable for numerous optoelectronics applications, ranging from solar cell and light-emitting devices to touch screens and photo-detectors,[17-21] but without the above mentioned instability of isolated layers of black phosphorus, which are highly hygroscopic (they tend to take up moisture from air) degrading in a few hours of exposition, which limits their application.[22,23]

Recent studies have shown both experimentally and theoretically that insights into the optical properties of few-layer antimonene based on Raman spectroscopy are hampered.[6,7] Tsai *et al.* synthesized multilayer antimonene on an InSb substrate by a plasma-assisted approach and

studied its photoluminiscence response, finding a peak that emerged at ~ 610 nm.[24] According to the authors, the as-synthesized multilayer antimonene was defective and non-continuous like a pile of multilayer nanoribbons uniformly distributed on the substrate, and they attributed this peak to a turbostratically-stacked nanoribbon structure and a quantum confinement effect.

In this work, we perform a combined characterization by atomic force microscopy (AFM) and quantitative optical microscopy of micromechanical exfoliated few-layer β antimonene (FL-Sb) crystals, as experimentally identified in ref. 6 (Figure 1 shows relevant views of the β-Sb phase atomic lattices).

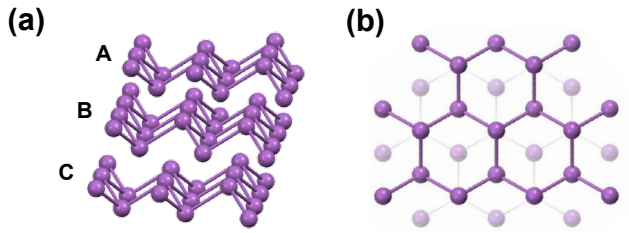

Figure 1. Relevant views of the β antimony atomic lattice. (a) 3D representation. (b) Top view.

We study the optical contrast dependence on the FL-Sb flakes as a function of their thickness and the illumination wavelength. From these measurements and using a simple model based on the Fresnel law, we obtain their refractive index and absorption coefficient in the visible spectrum (wavelengths ranging from 450 to 650 nm). The obtained values are in good agreement with theoretical calculations,[17,18] pointing towards antimonene as a suitable material for optoelectronic and photonic devices. Since Raman spectroscopy cannot be used for the identification of antimonene thin flakes, we have studied the optical contrast dependence with the flake thickness providing a simple, quick and quantitative procedure to identify the number of layers of antimonene using optical microscopy.

EXPERIMENTAL

Sample preparation. Bulk commercially available crystalline antimony material (99.9999 %, Smart Elements) was used. We followed a double step transfer strategy[4] to prepare FL-Sb flakes, as explained in ref. 6. The procedure starts by mechanical exfoliation of a macroscopic freshly cleaved crystal of antimony by repetitive pealing using adhesive tape and a first transfer of antimony sheets from the adhesive tape to a thin layer of viscoelastic polymer (Gelfilm from Gelpak). A second transfer is then performed by pressing the polymer against a SiO_2/Si substrate (300 nm oxide silicon grown thermally on a Si (111) crystal). This double step strategy allowed cleaner flakes deposition (since the tape is not pressed against the substrate there is less adhesive) and a higher yield of larger flakes on the silicon oxide substrate.

Optical microscopy. The quantitative measurements of the optical contrast of FL-Sb flakes were carried out with a Nikon Eclipse LV100 optical microscope using non-polarized illumination under normal incidence with a 50× objective (numerical aperture NA = 0.55). The illumination wavelength was selected by means of eight narrow band-pass filters (10 nm full width at half maximum FWHM) with central wavelengths 450, 500, 520, 546, 568, 600, 632 and 650 nm purchased from Edmund Optics.

Atomic force microscopy. AFM measurements were carried out in contact mode under ambient conditions using a Cervantes Full-mode AFM from Nanotec Electronica SL. WSxM software (www.wsxmsolutions.com) was employed for both data acquisition and image processing.[25,26] Contact mode AFM has been chosen to avoid possible artifacts in the flake thickness measurements.[27] OMCL-RC800PSA cantilevers (probe.olympus-global.com) with a

nominal spring constant of 0.39 Nm^{-1} and tip radius of 15 nm were employed. Low forces of ~ 1 nN were used for imaging to ensure that the flakes suffer no damage by the tip.

RESULTS AND DISCUSSION

Figure 2 shows optical and AFM characterization of FL-Sb flakes deposited onto a 300 nm SiO_2/Si substrate (Experimental Section for details). Optical microscopy enables quick identification of the flakes and their lateral size.

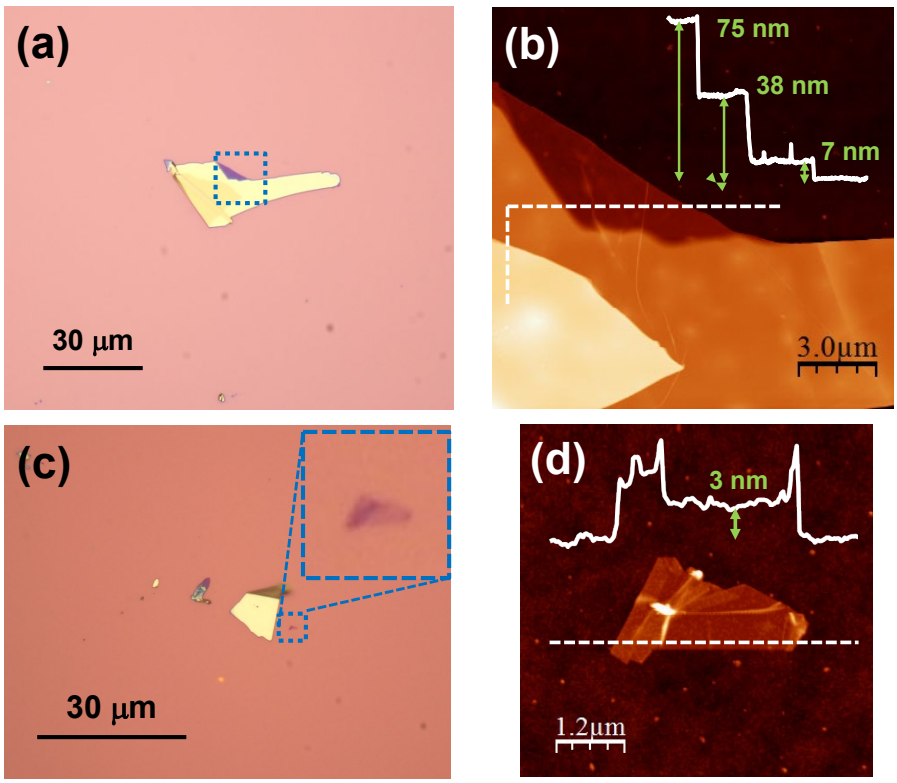

Figure 2. Optical and AFM characterization of FL-Sb flakes. (a) and (c) Optical microscopy images under white illumination of different FL-Sb flakes on a 300 nm SiO_2/Si surface. (b) and (d) are AFM topography images of the areas inside the dashed squares in (a) and (c) respectively. Inset profiles are taken along the dashed lines in the images.

In addition, it is possible to obtain an initial rough estimation of the thickness of the flakes due to a light interference effect, usually referred to as interference color.[28] AFM allows for a more accurate measurement of the thickness of the flakes. Different flakes with heights from tens of nm down to 2-3 nm (corresponding to ~ 4-7 layers) can be optically identified. AFM revealed smaller crystals down to the single- and bi- layer cases in the surroundings of the larger ones[6] but they were not large enough to be optically identified.

To study the optical contrast of these FL-Sb flakes an approach based on the Fresnel law similar to the one developed by Blake *et al.*[29] has been used. This method has been widely employed to study the optical contrast of different 2D crystals such as graphene,[29-31] transition metal dichalcogenides,[32-34] mica[35] or hexagonal boron nitride.[36]

We have quantitatively studied the optical contrast (C), which depends on the flake thickness (d) and the illumination wavelength (λ):

$$C(d,\lambda) = \frac{I_{flake} - I_{substrate}}{I_{flake} + I_{substrate}} \quad (1)$$

where I_{flake} and $I_{substrate}$ are the reflected light intensities from the flake and the SiO_2 substrate, respectively. The reflected intensity for normal incidence of monochromatic light can be written as:[29]

$$I_{flake}(d,\lambda) = \left| \frac{r_{01}e^{i(\Phi_1+\Phi_2)} + r_{12}e^{-i(\Phi_1-\Phi_2)} + r_{23}e^{-i(\Phi_1+\Phi_2)} + r_{01}r_{12}r_{23}e^{i(\Phi_1-\Phi_2)}}{e^{i(\Phi_1+\Phi_2)} + r_{01}r_{12}e^{-i(\Phi_1-\Phi_2)} + r_{01}r_{23}e^{-i(\Phi_1+\Phi_2)} + r_{12}r_{23}e^{i(\Phi_1-\Phi_2)}} \right|^2$$

$$I_{substrate}(d,\lambda) = \left| \frac{r_{02} + r_{23}e^{-2i\Phi_2}}{1 + r_{02}r_{23}e^{-2i\Phi_2}} \right|^2 \quad (2)$$

where the subindexes 0, 1, 2, and 3 refer to the media: air, FL-Sb flake, SiO_2, and Si, respectively. Fig. S1 in the Supporting Information shows a schematic diagram of the experimental setup. $\tilde{n}_j(\lambda) = n_j - i\kappa_j$ is the complex refractive index of the medium j, $\Phi_j = 2\pi\tilde{n}_j d_j/\lambda$

is the phase shift introduced by the medium j, with d_j the thickness of this medium j, and $r_{jk} = (\tilde{n}_j - \tilde{n}_k)/(\tilde{n}_j + \tilde{n}_k)$ the amplitude of the reflected path in the interface between the media j and k. $I_{substrate}$ is obtained by considering that medium 1 is air instead of a flake. The SiO_2 layer of thickness d_2 is optically characterized by a wavelength-dependent refractive index n_2 (λ) with no imaginary part,[37] ranging from 1.465 at 450 nm to 1.456 at 650 nm. As the thickness of the Si layer is several orders of magnitude larger than SiO_2 layer, it can be considered as a semi-infinite film. It is optically characterized by a wavelength-dependent refractive index $\tilde{n}_3$ (λ),[37] ranging from 4.682 – 0.1491i at 450 nm to 3.847-0.016i at 650 nm. For a given wavelength we have two unknown variables n_1 and κ_1 and a number of equations that is the number of measured thicknesses. The solution of this system is, therefore, overdetermined and we use least-squares fitting to find out $\tilde{n}_1$ (λ). Since least-squares fitting can sometimes lead to different solutions with similar convergence criteria (this is a well-known problem in fitting methods), in these cases we have chosen the solutions that best match the contrast observed in the optical images.

More in detail, we have analyzed the optical contrast of 10 antimony flakes with thicknesses ranging from d_1 = 2 up to d_1 = 100 nm (~ 4 to 270 layers), under a well-defined illumination wavelength using narrowband optical filters spanning the visible spectrum (Experimental Section for details). Figure 3 shows optical microscopy images of several flakes under white illumination (Figure 3(a)) and under selected wavelengths (Figure 3(b)-(e)).

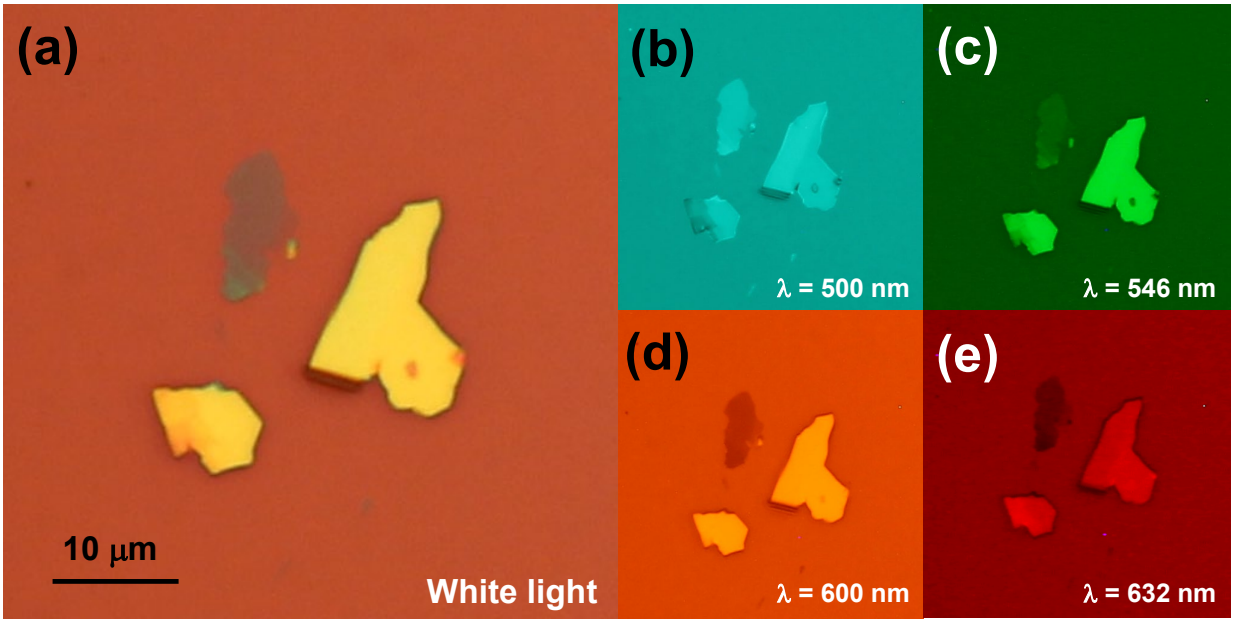

Figure 3. Different optical images acquired by using white light (a) and by using narrow bandwidth filters ((b)-(e), 500, 546, 600 and 632 nm respectively).

The measured optical contrast versus thickness for the four wavelengths in Figure 3 is shown in Figure 4. Optical contrast accurately follows eqs (1) and (2). Solid lines correspond to fits to the Fresnel law choosing the few-layer antimonene complex refractive index values that best fit (within the criterion above mentioned) the experimental data for each wavelength.

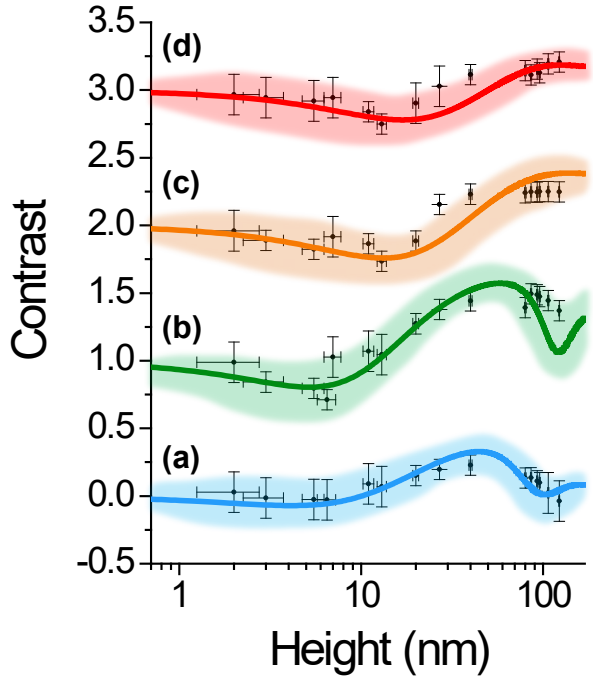

Figure 4. Measured optical contrast (small dot symbols) of few-layer antimonene flakes onto a 300 nm SiO_2 substrate versus their thickness from AFM measurements at different illumination wavelengths λ (nm): 500 (a), 546 (b), 600 (c), and 632 (d). Solid lines and shaded areas are the contrast and its uncertainty obtained from the fit to the Fresnel law. Note that (b), (c), and (d) have been vertically displaced for the sake of clarity by 1, 2, and 3 units, respectively.

The complex refractive index for FL-Sb obtained from similar fits as in Figure 4 at different illumination wavelengths is shown in Figure 5. Figure 5(a) shows both real (n, refractive index) and imaginary (κ, extinction coefficient) parts of the FL-Sb complex refractive index in the visible spectrum. Figure 5(b) shows the absorption coefficient, which is obtained from the extinction coefficient using the relation $\alpha = 4\pi\kappa/\lambda$[38] and it is usually expressed in cm^{-1}. The

absorption coefficient describes the decay of light intensity which traverses through the unit distance in a medium.

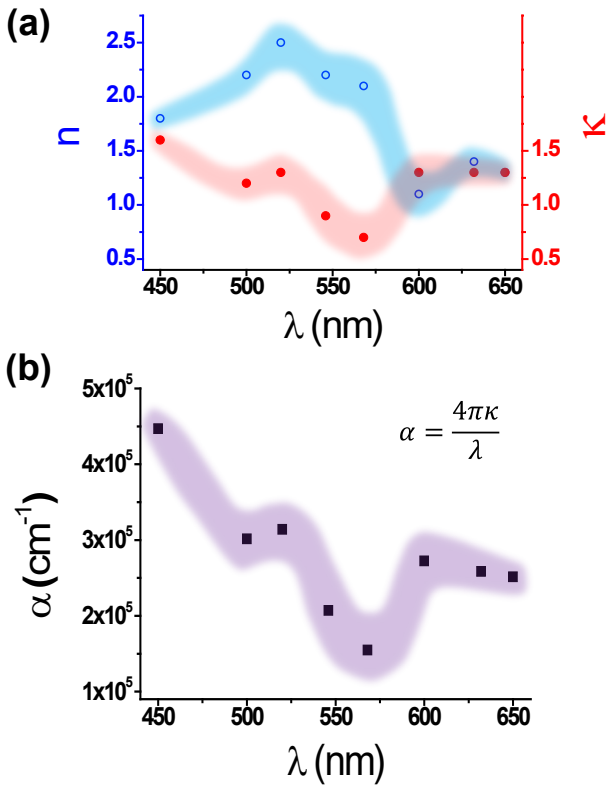

Figure 5. (a) Determined refractive index (blue open circles, left axis) and extinction coefficient (red filled circles, right axis) for FL-Sb as a function of the incident wavelength. (b) Determined absorption coefficient (black filled squares) for FL-Sb as a function of the incident wavelength. In both (a) and (b) the shaded areas represent the uncertainty of the data.

Our results for the complex refractive index and absorption coefficient as a function of the wavelength are in good agreement with previous theoretical calculations of these magnitudes for single layer antimonene performed over broader spectrum ranges[17,18]: the refractive index, n, in the visible range is around 1.5 and the extinction coefficient, κ, around 1.2. Both magnitudes

calculated for single layer antimonene[17,18] show similar dispersion relations despite lower values for the extinction coefficient. It is interesting to notice the behavior of the absorption coefficient, α, showing an increase from the IR to the UV zone, starting more markedly from a resonance at $\lambda \sim 580$ nm. This tendency of the absorption process is predicted by the theoretical calculations, starting in the IR part of the spectrum and peaking in the UV part. To gain further insight into the physical origin of the observed behavior, a simple analytical model can be applied to describe the dispersion relation of the obtained complex refractive index. We have used the two-pole Sellmeier equation,[39] resulting in an absorption resonance around 580-600 nm (in good agreement with that observed in the absorption coefficient, α), that points to the presence of a gap of electronic absorption around these values (Supporting Information for details).

In order to determine optimal conditions for the optical identification of ultrathin antimonene layers we have plotted the calculated contrast as a function of incident light wavelength and SiO_2 thickness (Figure 6). We define as optimal conditions for the optical identification the combination of wavelength and thickness that maximizes the absolute values of the layer contrast. To this end, we have used the obtained complex refractive index of FL-Sb to calculate the optical contrast of antimonene flakes, considering a thickness of 3.73 Å for the monolayer.[6] Albeit quantum confinement and/or excitonic effects can affect the optical properties, the use of the here reported complex refractive index can help to find the optimal conditions to visualize single and bilayer antimonene crystals. This has been reported in the literature with other monolayer materials, where the refractive index of the bulk has been successfully applied to study the optical properties of ultrathin crystals, including materials presenting band gap dependence with the number of layers.[29,32,40]

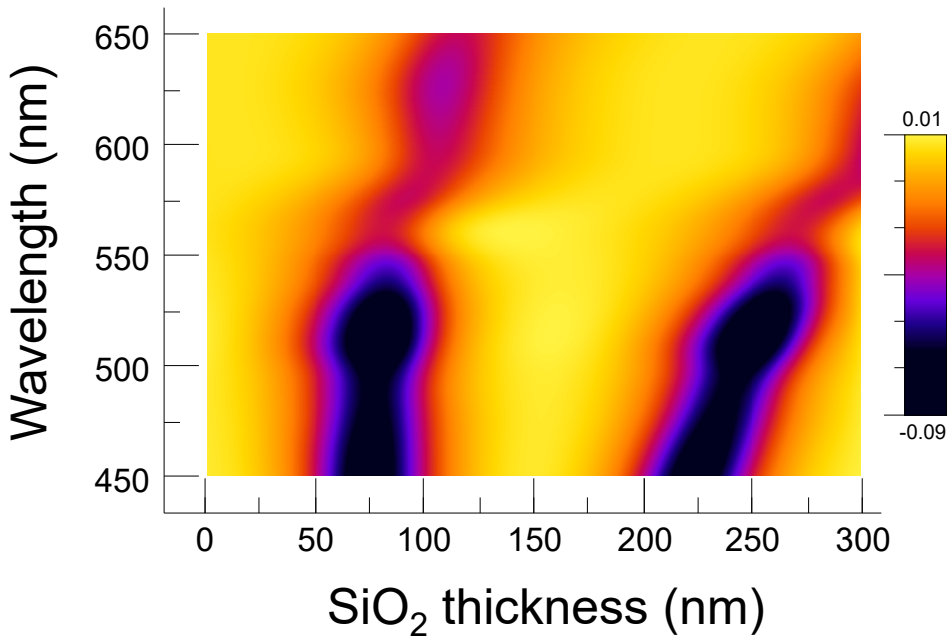

Figure 6. Optical contrast as a function of incident light wavelength and SiO_2 layer thickness for antimonene.

Figure 6 shows two characteristic negative contrast bands centered at thicknesses of 80 and 230 nm (at 450 nm wavelength) that shift towards higher thicknesses with increasing wavelength. In particular, the highest contrasts are found for thicknesses around 80 and 220-250 nm at wavelengths below 550 nm. For the case of the two most commonly used substrates, 90 and 300 nm of SiO_2 thickness, whereas the wavelengths for the 90 nm substrates are very similar as for the optimal 80 nm case, for the 300 nm thickness (the thickness used in the present study) the optimal wavelength is ~ 580 nm. This wavelength is, indeed, close to the one which the human eye has maximum sensitivity, ~ 562 nm,[41] which might help to detect the lower terraces when using this oxide thickness substrates. In this case, the use of light illumination at this wavelength will ease the optical identification of ultrathin antimonene layers (Fig. S3a,c in the

Supporting Information). A similar contrast plot has been obtained estimating theoretical (n, k) values for monolayer antimonene in the visible region from ref. 17 (Fig. S3b). Despite a decrease in the contrast magnitude, the observed trend is similar, presenting the same two characteristic negative contrast bands as in Figure 6, leading to similar optimal conditions.

CONCLUSIONS

We have studied the dependence of the optical contrast with the flake thickness and the illumination wavelength of few-layer antimonene flakes on SiO_2/Si substrates produced by mechanical exfoliation of bulk antimony crystals. From the contrast versus thickness measurements and applying a Fresnel-law based model we have determined the refractive index and the absorption coefficient in the visible spectrum of these ultrathin antimonene flakes. The obtained values are in good agreement with theoretical calculations, pointing towards antimonene as a suitable material for optoelectronic and photonic applications. Since Raman spectroscopy fails to provide information on few-layer antimonene, we have demonstrated that optical microscopy can be used as a simple tool to identify ultrathin antimonene crystals and to distinguish them from thicker flakes. We have investigated the optimal combination of wavelength and SiO_2 thickness to better identify mono- or few-layer antimonene crystals when deposited in commonly used SiO_2/Si substrates. Thus, optical microscopy is a suitable technique to identify and determine the thickness of antimony flakes in a fast and non-destructive way. This work can be considered as a starting point towards deeper experimental studies of the optical properties of few-layer antimonene and will ease the integration of ultrathin antimonene crystals on future nanodevices.

AUTHOR INFORMATION

Corresponding Author

*P. Ares. E.mail: pablo.ares@uam.es; J. Gomez-Herrero. E-mail: julio.gomez@uam.es

Funding Sources

Funded by MINECO (Spain) through projects Consolider CSD2010-0024, MAT2016-77608-C3-1P and 3P.

ACKNOWLEDGMENT

We want to thank Gabino Rubio-Bollinger, Jorge Quereda and Andres Castellanos-Gomez for technical assistance. This work was supported by Consolider CSD2010-0024, MAT2016-77608-C3-1P and 3P.

ASSOCIATED CONTENT

Supporting Information

The Supporting Information is available free of charge on the ACS Publications website at DOI: 10.1021/acsphotonics.xxxxxxx

Schematic diagram of the experimental setup (PDF)

Sellmeier equation (PDF)

Optical contrast as a function of incident light wavelength and SiO_2 layer thickness from experimental and theoretical complex refractive indexes (PDF)

Optical images at white light and at different wavelengths (PDF)

.

REFERENCES

(1) Geim, A. K.; Novoselov, K. S. The rise of graphene. *Nat. Mater.* **2007**, *6*, 183-191.

(2) Mas-Balleste, R.; Gomez-Navarro, C.; Gomez-Herrero, J.; Zamora, F. 2D materials: to graphene and beyond. *Nanoscale* **2011**, *3*, 20-30.

(3) Novoselov, K. S.; Jiang, D.; Schedin, F.; Booth, T. J.; Khotkevich, V. V.; Morozov, S. V.; Geim, A. K. Two-dimensional atomic crystals. *Proc. Nat. Acad. U.S.A.* **2005**, *102*, 10451-10453.

(4) Castellanos-Gomez, A.; Vicarelli, L.; Prada, E.; Island, J. O.; Narasimha-Acharya, K. L.; Blanter, S. I.; Groenendijk, D. J.; Buscema, M.; Steele, G. A.; Alvarez, J. V.; Zandbergen, H. W.; Palacios, J. J.; van der Zant, H. S. J. Isolation and characterization of few-layer black phosphorus. *2D Materials* **2014**, *1*, 025001.

(5) Li, L.; Yu, Y.; Ye, G. J.; Ge, Q.; Ou, X.; Wu, H.; Feng, D.; Chen, X. H.; Zhang, Y. Black phosphorus field-effect transistors. *Nat. Nanotech.* **2014**, *9*, 372-377.

(6) Ares, P.; Aguilar-Galindo, F.; Rodríguez-San-Miguel, D.; Aldave, D. A.; Díaz-Tendero, S.; Alcamí, M.; Martín, F.; Gómez-Herrero, J.; Zamora, F. Mechanical Isolation of Highly Stable Antimonene under Ambient Conditions. *Adv. Mater.* **2016**, *28*, 6332-6336.

(7) Gibaja, C.; Rodríguez-San-Miguel, D.; Ares, P.; Gómez-Herrero, J.; Varela, M.; Gillen, R.; Maultzsch, J.; Hauke, F.; Hirsch, A.; Abellán, G.; Zamora, F. Few-Layer Antimonene by Liquid-Phase Exfoliation. *Angew. Chem. Int. Ed.* **2016**, *55*, 14345-14349.

(8) Ji, J. P.; Song, X. F.; Liu, J. Z.; Yan, Z.; Huo, C. X.; Zhang, S. L.; Su, M.; Liao, L.; Wang, W. H.; Ni, Z. H.; Hao, Y. F.; Zeng, H. B. Two-dimensional antimonene single crystals grown by van der Waals epitaxy. *Nat. Commun.* **2016**, *7*, 13352.

(9) Wu, X.; Shao, Y.; Liu, H.; Feng, Z.; Wang, Y. L.; Sun, J. T.; Liu, C.; Wang, J. O.; Liu, Z. L.; Zhu, S. Y.; Wang, Y. Q.; Du, S. X.; Shi, Y. G.; Ibrahim, K.; Gao, H. J. Epitaxial Growth and Air-Stability of Monolayer Antimonene on PdTe2. *Adv. Mater.* **2016***,* 1605407.

(10) Akturk, O. U.; Ozcelik, V. O.; Ciraci, S. Single-layer crystalline phases of antimony: Antimonenes. *Phys. Rev. B* **2015**, *91*, 235446.

(11) Zhang, S.; Yan, Z.; Li, Y.; Chen, Z.; Zeng, H. Atomically Thin Arsenene and Antimonene: Semimetal-Semiconductor and Indirect-Direct Band-Gap Transitions. *Angew. Chem. Int. Ed.* **2015**, *54*, 3112-3115.

(12) Zhang, S. L.; Xie, M. Q.; Li, F. Y.; Yan, Z.; Li, Y. F.; Kan, E. J.; Liu, W.; Chen, Z. F.; Zeng, H. B. Semiconducting Group 15 Monolayers: A Broad Range of Band Gaps and High Carrier Mobilities. *Angew. Chem. Int. Ed.* **2016**, *55*, 1666-1669.

(13) Pizzi, G.; Gibertini, M.; Dib, E.; Marzari, N.; Iannaccone, G.; Fiori, G. Performance of arsenene and antimonene double-gate MOSFETs from first principles. *Nat. Commun.* **2016**, *7*, 12585.

(14) Wang, Y.; Ding, Y. Electronic Structure and Carrier Mobilities of Arsenene and Antimonene Nanoribbons: A First-Principle Study. *Nanoscale Res. Lett.* **2015**, *10*, 1-10.

(15) Yao, G.; Luo, Z.; Pan, F.; Xu, W.; Feng, Y. P.; Wang, X.-s. Evolution of Topological Surface States in Antimony Ultra-Thin Films. *Sci. Rep.* **2013**, *3*, 2010.

(16) Zhao, M.; Zhang, X.; Li, L. Strain-driven band inversion and topological aspects in Antimonene. *Sci. Rep.* **2015**, *5*, 16108.

(17) Singh, D.; Gupta, S. K.; Sonvane, Y.; Lukacevic, I. Antimonene: a monolayer material for ultraviolet optical nanodevices. *J. Mater. Chem. C* **2016**, *4*, 6386-6390.

(18) Xu, Y.; Peng, B.; Zhang, H.; Shao, H.; Zhang, R.; Lu, H.; Zhang, D. W.; Zhu, H. First-principle calculations of phononic, electronic and optical properties of monolayer arsenene and antimonene allotropes. *arXiv:*1604.03422 **2016**.

(19) Bonaccorso, F.; Sun, Z.; Hasan, T.; Ferrari, A. C. Graphene photonics and optoelectronics. *Nat. Photon.* **2010**, *4*, 611-622.

(20) Cheng, R.; Li, D.; Zhou, H.; Wang, C.; Yin, A.; Jiang, S.; Liu, Y.; Chen, Y.; Huang, Y.; Duan, X. Electroluminescence and Photocurrent Generation from Atomically Sharp WSe2/MoS2 Heterojunction p-n Diodes. *Nano Lett.* **2014**, *14*, 5590-5597.

(21) Ingrosso, C.; Bianco, G. V.; Corricelli, M.; Comparelli, R.; Altamura, D.; Agostiano, A.; Striccoli, M.; Losurdo, M.; Curri, M. L.; Bruno, G. Photoactive Hybrid Material Based on Pyrene Functionalized PbS Nanocrystals Decorating CVD Mono layer Graphene. *ACS Appl. Mater. Interfac.* **2015**, *7*, 4151-4159.

(22) Island, J. O.; Steele, G. A.; van der Zant, H. S. J.; Castellanos-Gomez, A. Environmental instability of few-layer black phosphorus. *2D Materials* **2015**, *2*, 011002.

(23) Moreno-Moreno, M.; Lopez-Polin, G.; Castellanos-Gomez, A.; Gomez-Navarro, C.; Gomez-Herrero, J. Environmental effects in mechanical properties of few-layer black phosphorus. *2D Materials* **2016**, *3*, 031007.

(24) Tsai, H.-S.; Chen, C.-W.; Hsiao, C.-H.; Ouyang, H.; Liang, J.-H. The advent of multilayer antimonene nanoribbons with room temperature orange light emission. *Chem. Commun.* **2016**, *52*, 8409-8412.

(25) Gimeno, A.; Ares, P.; Horcas, I.; Gil, A.; Gomez-Rodriguez, J. M.; Colchero, J.; Gomez-Herrero, J. 'Flatten plus': a recent implementation in WSxM for biological research. *Bioinformatics* **2015**, *31*, 2918-2920.

(26) Horcas, I.; Fernandez, R.; Gomez-Rodriguez, J. M.; Colchero, J.; Gomez-Herrero, J.; Baro, A. M. WSXM: A software for scanning probe microscopy and a tool for nanotechnology. *Rev. Sci. Instrum.* **2007**, *78*, 013705.

(27) Nemes-Incze, P.; Osvath, Z.; Kamaras, K.; Biro, L. P. Anomalies in thickness measurements of graphene and few layer graphite crystals by tapping mode atomic force microscopy. *Carbon* **2008**, *46*, 1435-1442.

(28) Kvavle, J.; Bell, C.; Henrie, J.; Schultz, S.; Hawkins, A. Improvement to reflective dielectric film color pictures. *Opt. Express* **2004**, *12*, 5789-5794.

(29) Blake, P.; Hill, E. W.; Castro Neto, A. H.; Novoselov, K. S.; Jiang, D.; Yang, R.; Booth, T. J.; Geim, A. K. Making graphene visible. *Appl. Phys. Lett.* **2007**, *91*, 063124.

(30) Jung, I.; Pelton, M.; Piner, R.; Dikin, D. A.; Stankovich, S.; Watcharotone, S.; Hausner, M.; Ruoff, R. S. Simple approach for high-contrast optical imaging and characterization of graphene-based sheets. *Nano Lett.* **2007**, *7*, 3569-3575.

(31) Roddaro, S.; Pingue, P.; Piazza, V.; Pellegrini, V.; Beltram, F. The optical visibility of graphene: Interference colors of ultrathin graphite on SiO2. *Nano Lett.* **2007**, *7*, 2707-2710.

(32) Benameur, M. M.; Radisavljevic, B.; Heron, J. S.; Sahoo, S.; Berger, H.; Kis, A. Visibility of dichalcogenide nanolayers. *Nanotechnology* **2011**, *22*, 125706.

(33) Castellanos-Gomez, A.; Agrait, N.; Rubio-Bollinger, G. Optical identification of atomically thin dichalcogenide crystals. *Appl. Phys. Lett.* **2010**, *96*, 213116.

(34) Castellanos-Gomez, A.; Navarro-Moratalla, E.; Mokry, G.; Quereda, J.; Pinilla-Cienfuegos, E.; Agrait, N.; van der Zant, H. S. J.; Coronado, E.; Steele, G. A.; Rubio-Bollinger, G. Fast and reliable identification of atomically thin layers of TaSe2 crystals. *Nano Res.* **2013**, *6*, 191-199.

(35) Castellanos-Gomez, A.; Wojtaszek, M.; Tombros, N.; Agrait, N.; van Wees, B. J.; Rubio-Bollinger, G. Atomically Thin Mica Flakes and Their Application as Ultrathin Insulating Substrates for Graphene. *Small* **2011**, *7*, 2491-2497.

(36) Gorbachev, R. V.; Riaz, I.; Nair, R. R.; Jalil, R.; Britnell, L.; Belle, B. D.; Hill, E. W.; Novoselov, K. S.; Watanabe, K.; Taniguchi, T.; Geim, A. K.; Blake, P. Hunting for Monolayer Boron Nitride: Optical and Raman Signatures. *Small* **2011**, *7*, 465-468.

(37) Palik, E. D. *Handbook of Optical Constants of solids*, San Diego, 1998.

(38) Hecht, E. *Optics*, Addison-Wesley: Boston, 2001.

(39) Ghosh, G.; Endo, M.; Iwasalu T. Temperature-Dependent Sellmeier Coefficients and Chromatic Dispersions for Some Optical Fiber Glasses. *J. Lightwave Technol.* **1994**, *12*, 1338-1342.

(40) Brotons-Gisbert, M.; Sánchez-Royo, J.F.; Martínez-Pastor J.P. Thickness identification of atomically thin InSe nanoflakes on SiO2/Si substrates by optical contrast analysis. *Appl. Surf. Sci.* **2015**, *354*, 453-458.

(41) Wald, G. Human Vision and the Spectrum. *Science* **1945**, *101*, 653-658.

TOC GRAPHIC